

ESRF-DOUBLE CRYSTAL MONOCHROMATOR PROTOTYPE - CONTROL CONCEPT*

M. Brendike, G. Berruyer, H. Gonzalez, L. Ducotté, C. Guilloud, M. Perez, R. Baker,
 ESRF – The European Synchrotron, Grenoble, France

Abstract

The ESRF-Double Crystal Monochromator (ESRF-DCM) has been designed and developed in-house to enable spectroscopy beamlines to exploit the full potential of the ESRF-EBS upgrade. To reach concomitant beam positioning accuracy and beam stability at nanometer scale with a reliable, robust and simple control system, a double cascaded control architecture is implemented.

The cascade is comprised of three modes: classic open loop actuation, an optimized open loop mode with error mapping, and closed loop real-time actuation. Speedgoat hardware, programmable from MATLAB/SIMULINK and running at 10 kHz loop frequency is used for the real-time mode. From the EBS startup 2020, the ESRF plans to deploy BLISS – the new BeamLine Instrumentation Support Software control system – for running experiments. An interface between Speedgoat hardware and BLISS has therefore been developed. The DCM and its control architecture have been tested in laboratory conditions.

An overview of the concept, implementation and results of the cascaded control architecture and its three modes will be presented.

INTRODUCTION

Beamlines applying x-ray experimental techniques, such as x-ray absorption spectroscopy (XAS), are among the most demanding applications for monochromators. They need to scan through x-ray wavelengths (energies) quickly, in a repeatable manner, and without disturbing the position of the x-ray beam. Such ESRF beamlines are typically equipped with vertically-deflecting, fixed exit double crystal monochromators (DCMs), which allow to scan without readjustment of the downstream optical elements, or samples. The principle of a fixed exit DCM is explained in Fig. 1. Depending on the incident angle (Bragg angle, θ) of the beam on the first crystal an energy, E , can be selected. To maintain the reflected beam at the same height for all Bragg angles, θ , the second crystal needs to be adjusted relative to the position of the first. Current DCMs at the ESRF which follow this principle, are KOHZU monochromators as described in [1]. These DCMs keep the second crystal at the correct distance by a double cam mechanism. Since this is a purely mechanical process, second crystal positioning precision is limited. Prestipino et al. [2] proposed an active feedback system, called MOCO and later MOCO2 to compensate for mechanical errors. Although this improves results, limitations in terms of actuation bandwidth and usability for low energy XAS (such as ESRF-ID21) remain. As most of the current KOHZU DCMs were purchased around 20 years ago, ageing is a

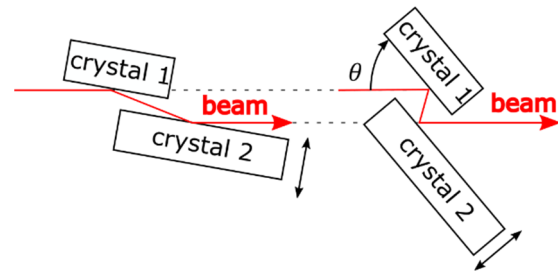


Figure 1: Principle of a fixed exit DCM; left at low Bragg angle; right at high Bragg angle.

major issue. In addition the ESRF-extremely brilliant source (EBS) upgrade will result in a more coherent and more intense light source [3]. The subsequent improvement in experimental techniques will further increase the demand in beam position stability and actuation bandwidth. These new requirements led to the decision of designing a new generation of DCMs in-house at the ESRF.

To exploit the potential of the new ESRF-EBS, monochromators need a second crystal positioning system that is simultaneously faster and more accurate than that of KOHZU DCMs. Baker et al [4] presented the mechanical concept of the ESRF-DCM prototype in 2018. Figure 2 shows the principle of the second crystal positioning system. While KOHZU DCMs use a double cam mechanism, the ESRF-DCM is equipped with a tripod positioning stage composed of three stepper motors, for the long stroke (in-

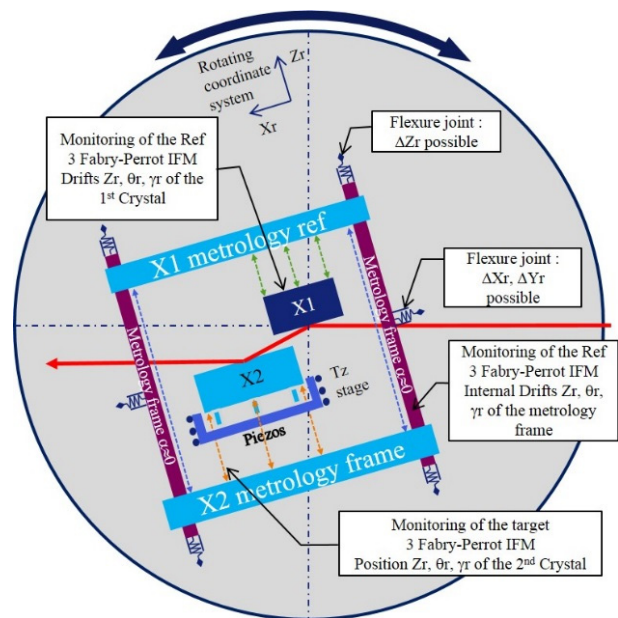


Figure 2: Online crystal metrology and second crystal actuation schema.

* **Authors contributions:** M.B. design and implementation; G.B., C.G. and M.P. implementation in BLISS and BLISS-RPC; H.G. electronics; L.D. concept of metrology and actuation; R.B. Project coordinator

Content from this work may be used under the terms of the CC BY 3.0 licence (© 2019). Any distribution of this work must maintain attribution to the author(s), title of the work, publisher, and DOI.

icated as Tz stage), and three piezo actuators, for fine adjustment. A metrology frame, consisting of 9 interferometers which observe the positions of the two crystals and drifts of the metrology frame itself, is used as a feedback system. Closing the feedback loop for the second crystal positioning system should result in an improved parallelism between the two crystals and hence a more stable energy and beam position at the sample.

A monochromator is one of the most important beamline instruments for spectroscopy applications. In the event of control system failures, the ESRF-DCM will no longer be able to function in fixed exit mode, and hence XAS measurements will be impossible. This underlines the importance of a reliable control system. Further a monochromator should be an easy to use instrument and therefore a simple and user friendly interface must be provided. These issues are considered, amongst others, in the control concept presented here.

ESRF-DCM CONTROL CONCEPT AND IMPLEMENTATION

A schematic design of the ESRF-DCM, its actuators and feedback systems, is given in Figure 3. The Bragg motor drives both crystals to the requested angular position. Simultaneously three internally linked stepper motors position the second crystal to approximately the correct position. Reading the current Bragg position and feedback from either the crystal parallelism or a beam position monitor, the real-time system corrects any residual errors using piezo actuators. To ensure operation in the case of a failure of the real-time system or its associated components, the ESRF-DCM and its control concept were designed following the principles presented in Figure 4.

Splitting the control system into three different modes ensures increased overall reliability, and simultaneously provides access to high actuation bandwidths and positioning accuracies if needed. Mode A (blue and left in Fig. 4) is the most robust and mode C (red and right in Fig. 4) is optimised for ultimate positioning accuracy. This principle

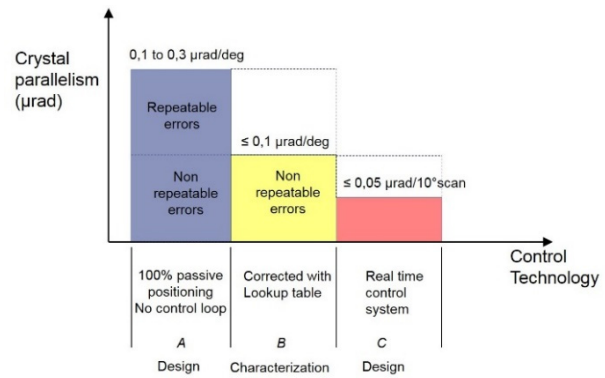


Figure 4: ESRF-DCM design principles and the resulting control modes A, B and C.

allows to switch between modes depending on the beamline’s needs and guarantees backup solutions in case of reliability issues.

The design principles shown in Fig. 4 translates into a block diagram as shown in Fig. 5. In the diagram the cascaded control architecture depending on the different modes becomes visible. The yellow-highlighted feedback loop (mode B) represents the first cascade. The red-highlighted loop (mode C) represents the second cascade. If both loops are opened, mode A is active, corresponding to a classic open loop control.

The full system is a three dimensional multiple input multiple output (MIMO) system, all the following equations are hence matrix equations.

Mode A contains an open loop actuation by stepper motors. It is based on the inverse kinematics of the second crystal tripod system and does not include any feedback system. Its transfer function is therefore given by

$$Y(s) = G_P(s) X(s) = \underbrace{G_P(s) G_{st}(s) H^{-1}}_{G_A(s)} R(s) . \quad (1)$$

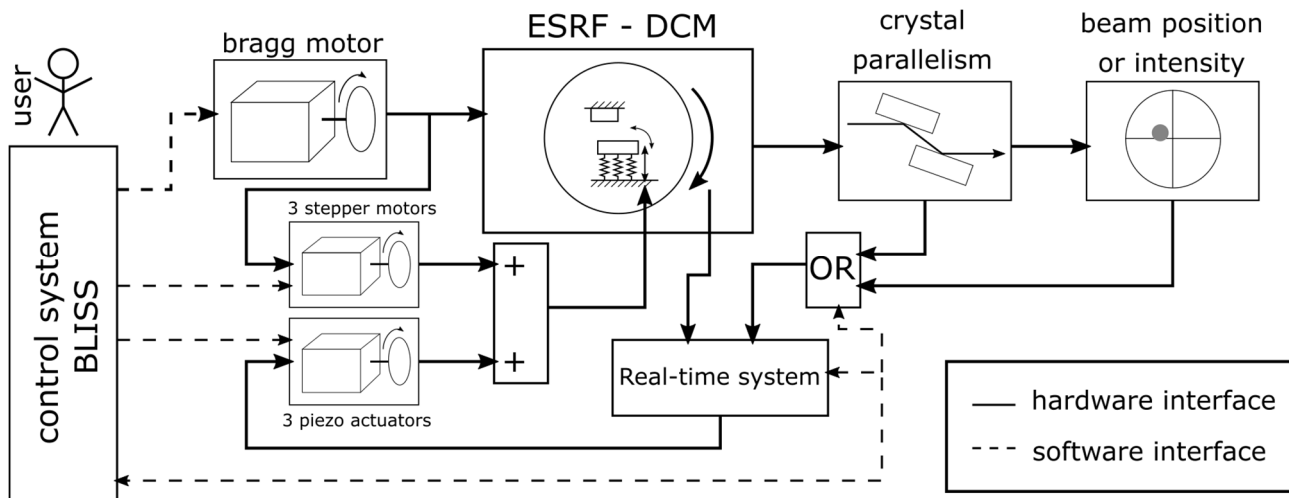


Figure 3: Schematic design of the control, actuators and feedback systems of the ESRF-DCM.

Content from this work may be used under the terms of the CC BY 3.0 licence (© 2019). Any distribution of this work must maintain attribution to the author(s), title of the work, publisher, and DOI.

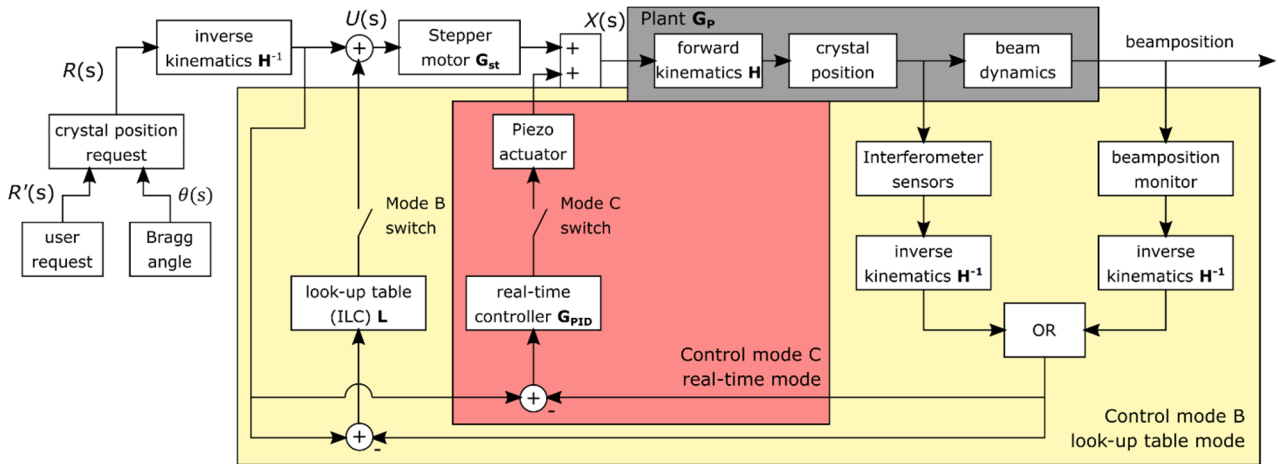


Figure 5: Block diagram of the ESRF-DCM control system.

Where $Y(s)$ is the beam position vector, $X(s)$ is the position vector (distance and orientation) of the second crystal, $R(s)$ is the requested position vector, $G_P(s)$ is the plant transfer function matrix, H^{-1} is the tripod's inverse kinematics matrix and $G_{st}(s)$ the transfer function matrix of the three stepper motors. Since there is no feedback loop and $G_{st}(s)$ and H^{-1} are asymptotically stable transfer functions, $G_A(s)$ is intrinsically asymptotically stable.

Mode B improves the positioning accuracy of the second crystal by using a first feedback loop. It is important to emphasize that, as the tripod positioning system has repeatable errors which need to be compensated by the use of look-up tables (see Fig. 4), this loop is not designed as a classical regulation loop, but rather as an iterative learning control (ILC). A monochromator is a central beamline instrument which must run for long periods with no intervention. It is inconceivable to transfer a DCM back into a laboratory and recalibrate the look-up tables every time the performance degrades. A learning control algorithm is therefore used to calibrate the look-up tables automatically while the DCM is in use and if feedback information is available. Mode B still works only with the tripod's in-vacuum stepper motors.

The implementation of mode B is slightly different from a standard control design in Laplace domain. A classic ILC, as presented by Longman [5] defines the starting point. We begin with the classic iterative learning law in time domain

$$\begin{aligned} \underline{u}_{j+1} &= \underline{u}_j + \underline{L}e_j \\ \underline{u}_j &= [u_j(0) \ u_j(1) \ \dots \ u_j(p-1)]^T \\ \underline{e}_j &= [e_j(1) \ e_j(2) \ \dots \ e_j(p)]^T, \end{aligned} \quad (2)$$

where $u_j(k)$ is the command control input at the time sample k at cycle j , $e_j(k+1)$ is the measured error at the sample $k+1$ at cycle j , L is the learning matrix and the time samples are given by $k = 0, 1, \dots, (p-1)$. Since we are only interested in error mapping over Bragg angle θ and not over time, we modify the law to

$$\begin{aligned} \underline{u}_{j+1} &= \underline{u}_j + \underline{L}e_j \\ \underline{u}_j &= [u_j(0) \ u_j(d\theta) \ \dots \ u_j((p-1)d\theta)]^T \\ \underline{e}_j &= [e_j(d\theta) \ e_j(2d\theta) \ \dots \ e_j(pd\theta)]^T. \end{aligned} \quad (3)$$

By using the inverted plant model as learning matrix L

$$L = \beta \hat{G}_p^{-1} \quad (4)$$

complete convergence can be reached in one step, if \hat{G}_p^{-1} is known and $\beta = 1$. Here \hat{G}_p is not the plant model transfer function but a Toeplitz matrix with the Markov parameters of $G_P(s)$. As Longman [5] shows, stability is given for $0 < \beta < 2$, which can be used as a tuning parameter for the learning algorithm.

A disadvantage of this approach is, that \hat{G}_p^{-1} must be known. For the analysed system, only the kinematics and no kinetics are modelled. Consequently stability and convergence of the learning algorithm are only ensured for quasi-static Bragg angle movements. If the Bragg movements provokes highly dynamic effects, this can result in destabilisation of the learning loop.

Mode C includes the real-time feedback system and uses piezo actuators to compensate the residual errors of the stepper motors run in mode B. For the moment a classic PID controller is used in the feedback loop of mode C. It is designed using classic open loop loop-shaping methods. The closed loop system results to be

$$Y(s) = \frac{G_{PID}G_P(I_3 + G_{PID}G_P)^{-1}H^{-1}}{G_C(s)} R(s). \quad (5)$$

Where $G_{PID}(s)$ is the transfer function matrix of the designed real-time controller and thus $G_C(s)$ the closed loop transfer function matrix for mode C. Currently the MIMO controller $G_{PID}(s)$ is implemented in a diagonal form

$$G_{PID}(s) = G_{PID}(s)I_3 \quad (6)$$

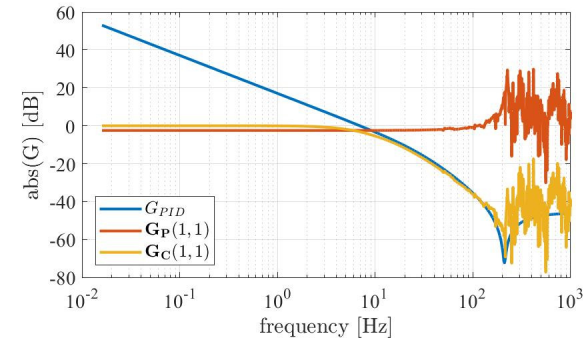


Figure 6: Singular value plot for the first entry of the transfer function of mode C $G_C(1,1)$ (yellow), the plant model $G_P(1,1)$ (red) and the PID controller $G_{PID}(s)$ (blue).

Where I_3 is the three dimensional identity matrix and $G_{PID}(s)$ is a single input single output (SISO) PID controller with a magnitude plot as shown in Fig. 6 in blue. Figure 6 also shows the first singular value of the plant model matrix $G_P(s)$ in red and of the closed loop system $G_C(s)$ in yellow. It can be seen that the closed loop system currently runs at a relatively low bandwidth of about 10 Hz. This is due to the fact that the dynamic system $G_P(s)$ follows a complex dynamic behaviour, and thus classic open loop loop-shaping methods are difficult to implement. Further investigations with closed loop loop-shaping methods and other control design methods are foreseen in the future to enhance the bandwidth of mode C.

Since mode B is not a regulation loop with active real-time feedback, it does not influence the stability of mode C. This can be explained as follows; the ILC changes only the position of the stepper motors from one cycle to another, during the cycle it remains constant. In other words, the ILC acts on the closed loop system $G_C(s)$ as a cyclic disturbance, and hence does not affect the stability properties of a closed loop system.

In both modes B and C the user has the option to select between two different feedback signals: either the interferometers, measuring directly the crystal parallelism inside the DCM, or an external beam position monitor. Both options have advantages and disadvantages, so that the users finally can decide themselves which signal they want to work with.

Implementation into the BeamLine Instrumentation Support Software control system, BLISS, is shown in Fig. 7. BLISS accesses all motor drivers (intelligent controller for positioning applications, ICEPAP), the real-time system, and all other beamline instruments. For direct communication between BLISS and the real-time control system a BLISS RPC server (remote procedure call) protocol has been developed. It is built on top of a python wrapping of the dynamic link library (DLL) provided with the real-time hardware from Speedgoat GmbH. By using this server, all parameters and signals inside the Speedgoat real-time system are directly accessible from BLISS.

Control mode A runs directly on the ICEPAP drivers, which synchronise the different motors. Mode B is run on

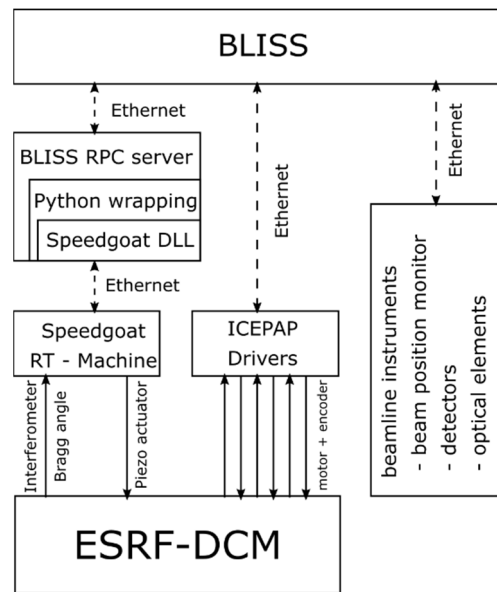


Figure 7: Implementation of drivers and real-time machine in the control system BLISS.

the level of the ICEPAP drivers and BLISS. BLISS gathers information concerning cyclic errors, from either the real-time system or other instruments, and reconfigures regularly the look-up tables used in the ICEPAP drivers. Control mode C runs locally on the real-time machine. To activate or deactivate control mode C BLISS can access a parameter on the real-time machine which closes or opens the feedback loop.

TEST RESULTS AND DISCUSSION

During the ESRF-EBS long shutdown and the consequent lack of a test beamline (December 2018 – February 2020), a laser setup was designed around the ESRF-DCM for laboratory tests. Figure 8 illustrates the setup. The laser passes through the monochromator, gets reflected on the two crystals and propagates onto two four quadrant diodes. By analysing the position of the reflected beam on the two diodes, beam position and orientation downstream of the ESRF-DCM can be analysed.

Figure 9 shows the beam stability observed, using the laser set-up, during a ten degree Bragg scan. It demonstrates that changing from mode A, to B, to C results in

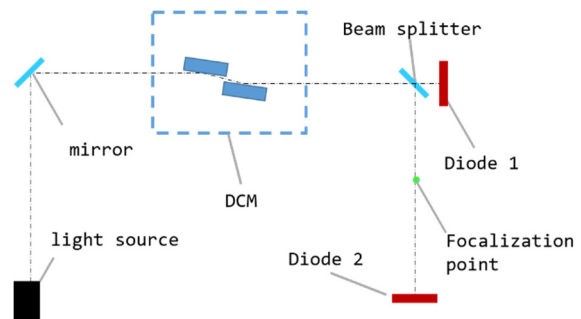


Figure 8: Concept of the laser setup for laboratory tests.

Content from this work may be used under the terms of the CC BY 3.0 licence (© 2019). Any distribution of this work must maintain attribution to the author(s), title of the work, publisher, and DOI.

improved beam stability. However, it appears that repeatable errors remain uncompensated in mode B. This can be improved further. Mode B uses only in-vacuum stepper motors, hence the positioning accuracy will stay limited due to stick-slip effects and nonlinearities inside the mechanics. Mode C shows very promising results. Figure 10 shows that in mode C there is little difference in beam stability between scanning through Bragg angles and not moving. In mode C it is the laser set-up stability that is the limiting factor when characterising the ESRF-DCM.

Further tests after the ESRF-EBS start-up will be necessary to define the final resolution in control mode B and C.

CONCLUSION

The control concept presented here respects the design principles of the ESRF-DCM. A cascaded control architecture with an ILC in the first cascade, and a PID controller in the second cascade is implemented. By automatically adapting look-up tables in the motor drivers the ILC minimises repeatable errors. The performance of mode C is further improved using active real-time control. This reduces both non-repeatable errors, and those repeatable errors which are too small to be compensated by mode B. The developed BLISS RPC Server allows the control system to access all information available on the Speedgoat real-time machine at any time.

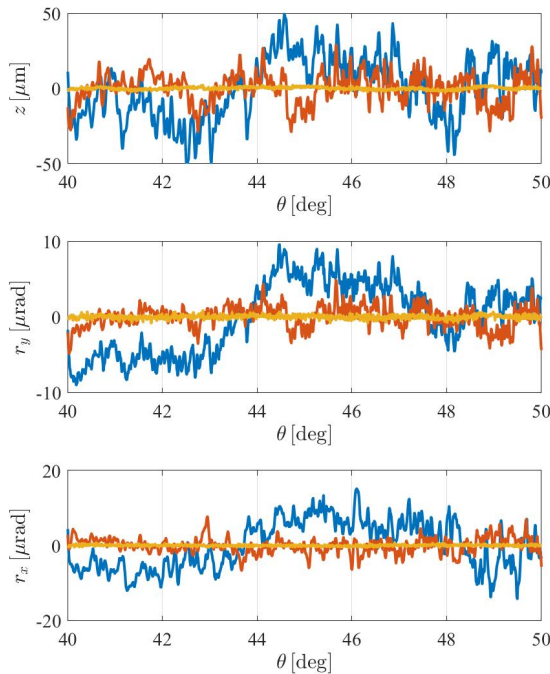


Figure 9: Beam stability of the reflected laser beam during a scan over the Bragg angle θ ; blue – Mode A; red – Mode B; yellow – Mode C.

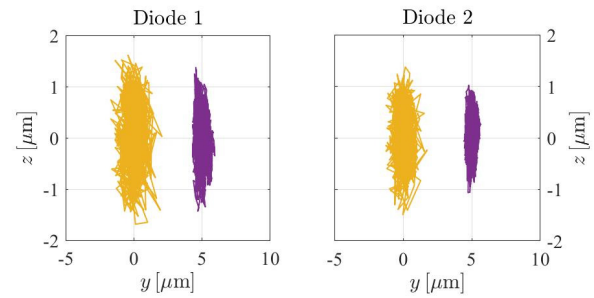


Figure 10: Laser spot position on the two diodes; during scan in mode C (yellow), and without scanning (purple).

While the initial results, obtained in laboratory test are promising, the final performance of the ESRF-DCM will only be characterised after the ESRF-EBS start-up. Current results indicate that it is the laser set-up resolution that limits the ESRF-DCM performance. The results presented here have been obtained by step-by-step scans, and provide little information on the dynamic performance of the system. Further work on the real-time controller, and the beamline control system (BLISS) will enable the system to be accurate both in step-by-step, and continuous scans.

ACKNOWLEDGEMENTS

The authors would like to express their special thanks to the beamline staff of ID21, J. BONNEFOY and N. SEVELIN-RADIGUET who made the installation of the laser setup possible.

REFERENCES

- [1] M. Cotte, E. Pouyet, M. Salomé *et al.*, "The ID21 X-ray and in-fared microscopy beamline at the ESRF: status and recent applications to artistic materials," *Journal of Analytical Atomic Spectrometry*, vol. 32, no. 3, pp 477-493, 2017.
- [2] C. Prestipino, O. Mathon, R. Hino *et al.*, "Quick-EXAFS implementation on the general purpose EXAFS beamline at ESRF," *Journal of Synchrotron Radiation*, vol. 18, no. 2, pp. 176-182, 2011.
- [3] The orange Book - ESRF UPGRADE PROGRAMME PHASE II (2015 - 2022), TECHNICAL DESIGN STUDY, http://www.esrf.fr/Apache_files/Upgrade/ESRF-orange-book.pdf
- [4] R. Baker *et al.*, "ESRF Double Crystal Monochromator Prototype Project", in *Proc. MEDSI'18*, Paris, France, Jun 2018, pp. 440-444. doi:10.18429/JACoW-MEDSI2018-FROAMA07
- [5] R. Longman, "Iterative learning control and repetitive control for engineering practice," *International Journal of Control*, vol. 73, no. 10, pp. 930-954, 2000.